

A SEARCH FOR X-RAY COUNTERPARTS OF GAMMA-RAY BURSTS WITH THE *ROSAT* PSPC

ALEXEY VIKHLININ

Harvard-Smithsonian Center for Astrophysics, 60 Garden St., Cambridge, MA 02138; avikhlinin@cfa.harvard.edu

ApJ Letters, in press

ABSTRACT

We search for faint X-ray bursts with duration 10–300 seconds in the *ROSAT* PSPC pointed observations with a total exposure of 1.6×10^7 s. We do not detect any events shorter than ~ 100 s, i.e. those that could be related to the classic gamma-ray bursts (GRB). At the same time, we detect a number of long flares with durations of several hundred seconds. Most, but not all, of the long flares are associated with stars. If even a small number of those long flares, that cannot identified with stars, are X-ray afterglows of GRB, the number of X-ray afterglows greatly exceeds the number of BATSE GRB. This would imply that the beaming factor of gamma-rays from the burst should be > 100 . The non-detection of any short bursts in our data constrains the GRB counts at the fluences 1–2.5 orders of magnitude below the BATSE limit. The constrained burst counts are consistent with the extrapolation of the BATSE $\log N - \log S$ relation. Finally, our results do not confirm a reality of short X-ray flashes found in the *Einstein* IPC data by Gotthelf, Hamilton and Helfand.

Subject headings: gamma-rays: bursts — surveys — X-rays: bursts

1. INTRODUCTION

Data accumulated over several years of observations by *ROSAT* and *Einstein* may contain X-ray counterparts of gamma-ray bursts (GRB). Both instruments have imaging capabilities and can provide precise positions leading to GRB identifications. Soft X-ray data can be used to constrain the $\log N - \log S$ distribution of gamma-ray bursts at fluxes below those accessible by BATSE. A possibility to find X-ray afterglows of gamma-ray bursts, similar to those recently discovered by BeppoSAX (Costa et al. 1997, Piro et al. 1998), is another motivation for a search for soft X-ray flares.

Gotthelf, Hamilton and Helfand (1996, GHH hereafter) reported a detection of 42 faint X-ray flashes in the *Einstein* IPC data. Those flashes have typical fluxes of $10^{-10} - 10^{-9}$ ergs cm^{-2} in the 0.2–3.5 keV energy band and a typical duration of $\lesssim 10$ s. Their detection rate corresponds to about million per year per whole sky. Flashes are not correlated with any known sources, including nearby galaxies.

We have performed a search for faint X-ray bursts in the pointed *ROSAT* PSPC observations. Using the imaging capabilities of *ROSAT*, we detect bursts as spatially localized spikes in the count rate with duration less than about 100 seconds. Our dataset covers 2.5 times larger area and has 1.1 times longer exposure than the GHH *Einstein* IPC dataset.

2. *ROSAT* DATA AND ANALYSIS

ROSAT mirrors focus soft X-rays in the 0.1–2.4 keV energy band. The prime detector, PSPC, covers a circular region with an area of 2.7 deg^2 . The mirror vignetting is approximately a parabolic function of the off-axis angle; it drops to 50% at the edge of the field of view (FOV). The angular resolution varies from $\sim 30''$ (FWHM) on-axis to $\sim 2'$ at the edge of the FOV. The on-axis effective area is 450 cm^2 at 1 keV. The PSPC background is dominated by cosmic X-rays (Snowden et al. 1992). The PSPC count rate is not saturated for source fluxes up to $\sim 1000 \text{ phot s}^{-1}$. These properties of the *ROSAT* PSPC are relevant for our work; for a detailed description, see Trümper (1983), Aschenbach (1988) and Pfeffermann et al. (1987).

We used *ROSAT* PSPC pointed observations with exposures

> 500 s. Pointings to clusters of galaxies and supernova remnants were excluded because extended emission from the target fills a significant part of the FOV and complicates the analysis. We also excluded all pointings in the direction of high Galactic absorption ($N_H > 10^{21} \text{ cm}^{-2}$), thus omitting all Galactic plane targets. These selections leave 2256 individual observations with the total exposure of 1.6×10^7 s.

Standard *ROSAT* data products have a list of good time intervals for each observation. These intervals exclude target occultations by the Earth, the spacecraft passages through the South Atlantic Anomaly and radiation belts, intervals of poor aspect solution, and all detected instrument malfunctions. As is advised in Snowden et al. (1994), we excluded time intervals with the master veto rate $> 170 \text{ cnt s}^{-1}$. The soft part of the PSPC bandpass ($E < 0.4 \text{ keV}$) is affected by higher background, poorer angular resolution, and the presence of “afterpulse” events (Plucinsky et al. 1993). We, therefore, used only the hard, 0.5–2 keV, energy band.

2.1. Burst Detection

An outline of our burst detection algorithm is as follows. We sort photons detected in the entire FOV according to their arrival time and divide the observation into sequences of n photons, advancing the sequence in steps of $n/2$ (that is, the sequences are overlapping). In each such sequence, we analyze the photon coordinates searching for spatial concentrations that would correspond to flashes from point-like sources. We use sequence widths, n , of 10, 15, 20, 25, 35, 45, and 60 photons, corresponding to time intervals of 7–40 s for the average *ROSAT* PSPC background of $\approx 1.4 \text{ cnt s}^{-1}$ in the whole FOV (Fig. 1). This matches well the duration of the classic gamma-ray bursts (e.g., Terekhov et al. 1994) and the reported *Einstein* flashes. To find spatial concentrations of photons within a sequence, we create an image in sky coordinates. For each image pixel, we count photons within the 90% power radius of the PSF, calculated as a function of the off-axis angle (Hasinger et al. 1993). If the number of photons within this radius exceeds the preselected detection threshold, we consider it a burst detection.

The optimal detection threshold depends on the off-axis an-

gle because the size of the detect cell varies. We set detection thresholds such that the probability of a false detection in the analyzed data (3.6×10^7 photons detected in the source-free regions) is small, 0.02, and that the distribution of false detections is uniform over the FOV. The false detection probabilities are derived from Monte-Carlo simulations of 5×10^9 photons randomly distributed inside the FOV. The thresholds vary from 4 photons for the shortest photon sequence and the inner region of the FOV, to 11 photons for the longest photon sequence and the edge of the FOV. If the derived thresholds are lowered by 1 photon, one would expect ~ 3 false detections in the whole analyzed data.

The use of the photon sequences of a fixed length rather than fixed time intervals greatly reduces a possibility of false detections during the intervals of high background usually caused by scattered solar X-rays. The count rate is not used for burst detection, therefore the high background does not cause false detections as long as it is relatively uniform over the detector. The sensitivity to long bursts is smaller during the high background intervals because the photon sequences span shorter time and hence contain a smaller fraction of the burst flux. Fortunately, high background occurs only in a small fraction of the total exposure (Fig. 1). The loss of sensitivity during these intervals is fully accounted for in our calculations of the detection efficiency.

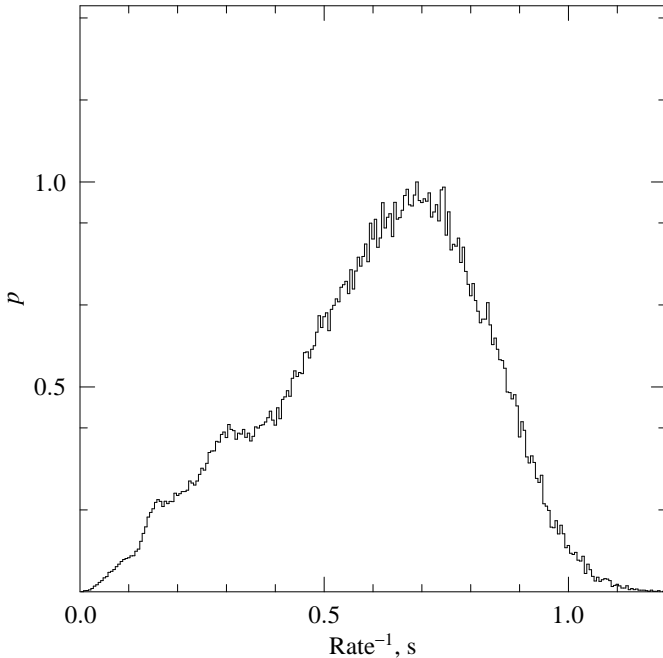


FIG. 1.— The distribution of the inverse *ROSAT* PSPC background rate in the whole FOV. The background rate was measured in sequences of 200 photons consecutively detected in source-free regions. The distribution represents the probability to measure a given count rate at a random moment in time.

Our burst detection algorithm requires absence of bright persistent sources. For example, if there is a source with the count rate equal to that of the background, 10 photons in each 20 photon sequence will be detected near the same position. This is above our threshold for burst detection. Even much fainter sources can increase the false detection probability. To avoid this problem, we masked all sources that were detectable in the image accumulated over the entire observation. Sources were detected using a matched filtering algorithm (Vikhlinin et al.

1995). Detection thresholds were 8–50 photons depending on the exposure and off-axis angle. Some of the detectable sources might be bright genuine bursts. To avoid missing such bursts, we analyzed light curves of all excluded sources.

2.2. Detection sensitivity

The probability to detect a burst of a given physical flux is a complex function of the burst flux, duration, off-axis angle, and the background intensity. It is also affected by the Poisson scatter of burst flux. The off-axis angle determines mirror vignetting and detection thresholds. Background rate and burst duration define a fraction of the burst flux within the n -photon sequence. To include all these effects into the burst detection probability, we used Monte-Carlo simulations. The burst position was simulated randomly inside the FOV. The burst flux was multiplied by the corresponding vignetting correction. The number of burst photons was simulated from the Poisson distribution. Photon positions were simulated according to the local PSF. Photon arrival times were simulated assuming an exponential light curve, $\exp(-t/t_0)$, with a random start time. The background intensity was simulated from the distribution in Fig 1. Positions of background photons were simulated according to the average PSPC exposure map. The burst detection algorithm was applied to the simulated data. Repeating the described simulations many times, we derived the probability to detect bursts of a given flux and duration.

Figure 2 shows the on-axis burst flux corresponding to an 80% detection probability as a function of burst duration T_{90} — time interval over which 90% of the burst flux is emitted. The limiting sensitivity varies slowly between 11 and 18 photons for $2 < T_{90} < 30$ s. For longer bursts, a significant fraction of flux is outside the longest photon sequence, and the limiting sensitivity correspondingly increases.

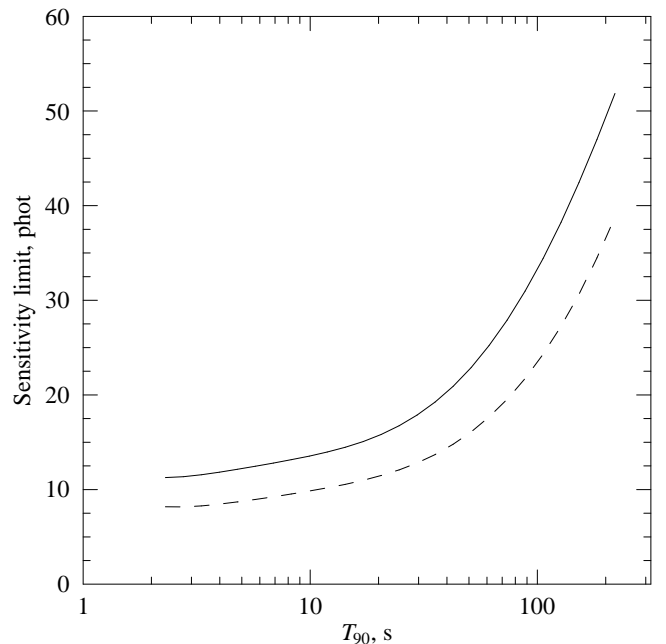


FIG. 2.— The on-axis burst flux corresponding to a 80% detection probability as a function of burst duration (solid line). The dashed line shows flux at which 37% of bursts are detected.

3. RESULTS

No bursts were found in the source-free regions¹. All bursts detected in the light curves of detected sources were longer than several hundred seconds (see below). Therefore, short, 10 s, flares similar to those detected by GHH in the *Einstein* data, were not found in any place of the *ROSAT* FOV. Our results clearly contradict to those of GHH and so a detailed comparison of the two searches must be made.

The total exposure of our *ROSAT* dataset, 1.6×10^7 s, is slightly longer than the *Einstein* exposure 1.5×10^7 s. The geometric area of the *ROSAT* PSPC FOV is 2.5 deg^2 , while the *Einstein* IPC covers only 1 deg^2 . In both instruments, the mirror vignetting is approximately parabolic and equals $\sim 50\%$ at the FOV edge; if anything, vignetting is more severe for the *Einstein* IPC. Therefore, our *ROSAT* data has an effective coverage (the product of exposure and the FOV area) 2.7 times larger than that of *Einstein*, which means that 2.7 more flares should be found in the *ROSAT* data, if the two searches have a similar sensitivity. GHH flares have $T_{90} < 10$ s. Our sensitivity limit for this duration is 14 photons. The average flux of GHH flares is 11 and 7 photons for “soft” and “hard” events, respectively. Since 37 out of 42 GHH flares were detected in the region where sensitivity is $< 60\%$ of that on-axis, the average on-axis flux is conservatively larger than 18.3 and 11.7 photons for “soft” and “hard” events, respectively. Our 0.5–2 keV energy band only partially overlaps with the *Einstein* energy band 0.16–3.5 keV used in GHH, and so conversion of count rates depends on the source spectrum. For sources with normal spectra, the *ROSAT* PSPC is more sensitive. For example, for $N_H = 10^{21} \text{ cm}^{-2}$ and a typical AGN spectrum with a photon index 1.5–2, the PIMMS software predicts the *ROSAT* count rate 1.3–1.5 times that of *Einstein*. GHH derive a photon index of ~ 2 for their hard flares, so we can conservatively assume that *ROSAT* count rates should be at least 30% higher for these events. For “soft” events, *ROSAT* sensitivity should be even higher. Therefore, we expect *ROSAT* on-axis fluxes of at least 23.8 and 15.2 photons for soft and hard flares, respectively. This is above our 80% sensitivity limit (Fig. 2), and so at least ~ 40 hard and ~ 50 soft flares are expected in the *ROSAT* data. To conclude, the discrepancy between *ROSAT* and *Einstein* cannot be explained by a difference in sensitivity.

We can offer only one astrophysical explanation of this discrepancy — a possibility of an unusual flare spectrum causing low *ROSAT* fluxes. One can estimate how unusual this spectrum should be. The 37% sensitivity limit, at which the sky coverage of our search becomes equal to that in GHH, corresponds to 10 photons for $T_{90} < 10$ s. To make the *ROSAT* flux below this limit, the *Einstein* count rate must be at least 1.2 times higher than that of *ROSAT*. This is only possible if the photon index is very small (< 0.5) or the spectrum is strongly self-absorbed ($N_H > 10^{22} \text{ cm}^{-2}$). We cannot exclude either flat spectrum or absorption, but they seem incompatible with the flare photon index of 2 derived by GHH.

3.1. Light curves of detectable sources

We also analyzed light curves of 93850 sources which were detected and excluded from our main burst search. The light curves were extracted within the 90% power radius around the source position. Source photons were binned into 10, 20, 40, ..., and 320 s time intervals. For a burst detection, we required that the peak flux exceeded 5 photons in a time bin, that the peak flux was at least three times higher than the average over

the observation, and that the Poisson probability of this deviation was less than 5×10^{-7} (i.e., a 5σ detection). These criteria correspond to a sensitivity approximately equal to the sensitivity of the burst detection in the source-free regions. *ROSAT* is routinely wobbled by $\pm 2-3'$ during the observation. The wobbling causes a spurious variability in a small fraction of the FOV attenuated by the window support structure of the PSPC. We excluded these regions from the source variability analysis. We also excluded 20% of the total exposure affected by high background.

We detected 141 bursts in the source light curves. The integral flux in these events was in the range 10–1000 photons. The quiescent flux was consistent with zero in approximately half of the bursting sources. All but one burst have $T_{90} > 200$ s. Examination of the Digitized Sky Survey (DSS) plates has shown that 112 bursting sources were Galactic stars. One burst comes from the X-ray binary LMC X-4. Dates and positions of the remaining 28 bursts are listed in Table 1. Many of these non-identified events still have star-like optical counterparts in the DSS, but the faintness of the counterpart (fainter than $\sim 16^m$) makes a reliable identification with Galactic stars impossible. Some bursting sources are probably extragalactic. Five of 28 flares are detected in the general direction of M31. The only short burst (8 photons in ~ 20 s) is located within the optical boundaries of M81. The peak luminosity in this event was $\approx 7 \times 10^{38} \text{ erg s}^{-1}$, assuming that it was located in M81 at $D = 3.5 \text{ Mpc}$. This was 40 times above the source quiescent luminosity, but only a small fraction, 4.5%, of the flux was emitted during the burst. These properties resemble Galactic X-ray bursters.

TABLE 1
LONG BURSTS WITHOUT A STELLAR IDENTIFICATION

Date (dd/mm/yy)	R.A. (J2000)	Decl. (J2000)	ID
05/07/91	00 31 26.5	+26 41 38	star-like
25/07/92	00 38 25.3	+31 23 50	uncertain
27/07/91	00 41 23.0	+41 49 08	uncertain
26/07/91	00 44 57.4	+41 59 25	star-like
10/01/93	00 45 31.4	+41 54 24	(a)
31/01/93	00 47 32.8	+42 50 03	star-like
25/07/91	00 49 47.9	+42 20 36	star-like
19/07/90	03 34 45.3	−25 37 27	star-like
27/03/92	05 28 11.8	−12 39 15	star-like
29/09/93	06 00 35.4	−38 50 25	uncertain
25/08/93	06 45 18.8	+82 48 23	star-like
22/08/93	07 14 36.3	+85 47 46	star-like
03/04/91	07 33 26.6	+31 44 08	star-like
29/09/93	09 55 26.5	+69 09 48	in M81
18/05/92	09 56 01.7	−05 12 41	star-like
11/05/93	10 34 09.4	+22 58 45	star-like
20/12/91	11 19 03.2	+07 49 27	star-like
30/12/91	12 35 30.0	+00 30 51	star-like
21/12/91	12 49 00.3	−06 28 09	star-like
03/02/93	13 38 15.1	−19 54 29	star-like
26/11/91	13 39 09.1	+48 21 10	star-like
02/07/94	13 41 21.6	+29 02 02	star-like
23/07/90	14 17 22.5	+25 05 16	star-like
23/01/92	15 04 18.8	+10 37 24	nothing
16/03/91	16 40 56.3	+70 42 38	star-like
07/08/93	16 39 51.1	+70 51 34	star-like
31/05/93	22 14 21.5	−16 53 56	uncertain
01/06/92	23 20 38.8	+08 21 09	star-like

^a — supersoft source in M31 (White et al. 1995)

A high quiescent flux of the short burst and long time scales

¹ Earlier versions of the *ROSAT* data processing contained an error which resulted in assigning the same $0.5''$ detector pixel to 5–30 consecutively detected photons. The *ROSAT* data do not contain this error any longer. We, however, were able to detect such “events” in some previously processed datasets.

of all other bursts indicate that the detected events are not related to X-ray flares detected by *Einstein*.

4. DISCUSSION

Ginga and BeppoSAX observations show that classic gamma-ray bursts are accompanied by a powerful, rapidly varying emission in the X-ray band (Yoshida et al. 1989, Frontera et al. 1998). We would detect this emission if the GRB had fallen inside the *ROSAT* FOV. Therefore, the non-detection of any short events in our *ROSAT* can be used to constrain the burst counts at a flux limit below that accessible by BATSE. A non-detection of any events in our search translates to a 90% upper limit of 7.2×10^4 bursts per year in the whole sky. Our limiting fluence is ~ 20 photons for $T_{90} \sim 10-100$ s. This corresponds to 2.6×10^{-10} erg cm $^{-2}$ in the 0.5–2 keV band, conservatively assuming the maximum absorption $N_H = 10^{21}$ cm $^{-2}$ in all pointings, and a 0.5–2 keV photon index $\Gamma = 1$, consistent with the average X-ray spectrum of Ginga bursts and the BeppoSAX spectrum of GRB 970508. The average ratio of 50–300 keV and 0.5–2 keV fluxes of Ginga gamma-ray bursts is ~ 60 (Yoshida et al. 1989²). BeppoSAX spectrum of GRB 970508 (Frontera et al. 1998) yields a 50–300/0.5–2 keV flux ratio of ~ 15 for a primary, hard pulse, and ~ 1 for a secondary, soft pulse. This range of observed GRB spectra corresponds to a limiting 50–300 keV fluence of 2.6×10^{-10} – 1.5×10^{-8} erg cm $^{-2}$ for our search. This is a 2.5–1 orders of magnitude improvement in sensitivity over BATSE (Fig 3).

With the present data, we cannot exclude a possibility that some of the detected long flares are X-ray afterglows of gamma-ray bursts, similar to those detected by BeppoSAX. We consider this possibility unlikely, mainly because 112 out of 141 these events are confidently identified with Galactic stars. Of the remaining 28 events, 27 have optical counterparts in the Digitized Sky Survey plates obtained years before the X-ray event. This is quite different from the properties of the optical transients associated with BeppoSAX GRB. For example, the 970508 transient was $R = 19.8$ in the maximum, that is, below or just at the limit of the DSS sensitivity. Therefore, flaring stars or perhaps AGN is a likely nature of the detected long flares. If, however, just several of them are indeed GRB afterglows, an immediate

implication is that gamma-ray bursts are highly collimated, because the long X-ray flares occur at a rate $\sim 10^5$ per year compared to the BATSE rate of ~ 700 GRB per year and because in X-rays, we do not see main bursts in the long flares.

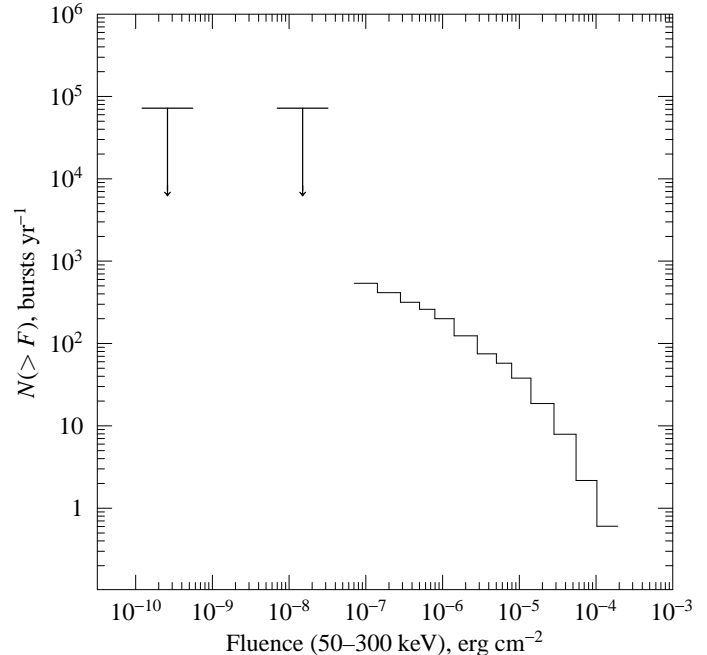


FIG. 3.— The log N –log S distribution for gamma-ray bursts. The histogram shows BATSE burst counts from Petrosian & Lee (1996). Upper limits correspond to a non-detection of soft X-ray bursts by *ROSAT*. High and low flux points correspond to the average Ginga GRB spectrum and to the BeppoSAX spectrum of GRB 970508, respectively (see text).

This work was supported by the Smithsonian Institution postdoctoral fellowship and the RBRF grant 95-02-05933. The author thanks R. A. Sunyaev for the encouragement of this work, and M. Markevitch, W. Forman, P. Gorenstein, and H. Tananbaum for interesting discussions.

REFERENCES

- Aschenbach, B. 1988, *Appl. Opt.*, 27, 1404
 Costa, E., et al. 1997, *IAU Circ.* 6572
 Frontera, F. et al. 1998, *ApJ*, 493, L67
 Gotthelf, E. V., Hamilton, T. T., & Helfand, D. J. 1996, *ApJ*, 466, 779 (GHH)
 Hasinger, G., Boese, G., Predehl, P., Turner, T., Yusaf, R., George, I., & Rohrbach, G. 1993, *GSFC OGIP Calibration Memo CAL/ROS/93-015*
 Petrosian, V., & Lee, T. T. 1996, *ApJ*, 467, L29
 Pfeffermann, E., et al. 1987, *Proc. SPIE*, 733, 519
 Piro, L., et al. 1998, *A&A*, 331, L41
 Plucinsky, P. P., Snowden, S. L., Briel, U. G., Hasinger, G., & Pfeffermann, E. 1993, *ApJ*, 418, 519
 Snowden, S. L., Plucinsky, P. P., Briel, U., Hasinger, G., & Pfeffermann, E. 1992, *ApJ*, 393, 819
 Snowden, S. L., McCammon, D., Burrows, D. N. & Mendehall, J. A. 1994, *ApJ*, 424, 714
 Terekhov, O., et al. 1994, *Astronomy Letters*, 20, 323
 Trümper, J. 1983, *Adv. Space Res.*, 2(4), 241
 Vikhlinin, A., Forman, W., Jones, C., & Murray, S. 1995, *ApJ*, 451, 553
 White, N. E., Giommi, P., Heise, J., Angelini, L., & Fantasia, S. 1995, *ApJ*, 445, L125
 Yoshida, A., et al. 1989, *PASJ*, 41, 509

²To calculate this number, we converted 1.5–10/1.5–375 keV flux ratios provided by Yoshida et al. into 0.5–2/50–300 keV flux ratios assuming a thermal bremsstrahlung spectrum